nature materials

LETTERS

PUBLISHED ONLINE: XX MONTH XXXX | DOI: 10.1038/NMAT4359

Time-domain separation of optical properties from structural transitions in resonantly bonded materials

Lutz Waldecker[1†], Timothy A. Miller[2†], Miquel Rudé[2], Roman Bertoni[1], Johann Osmond[2], Valerio Pruneri[2,3], Robert E. Simpson[4], Ralph Ernstorfer[1*] and Simon Wall[2*]

The extreme electro-optical contrast between crystalline and amorphous states in phase-change materials is routinely exploited in optical data storage[1] and future applications include universal memories[2], flexible displays[3], reconfigurable optical circuits[4,5], and logic devices[6]. Optical contrast is believed to arise owing to a change in crystallinity. Here we show that the connection between optical properties and structure can be broken. Using a combination of single-shot femtosecond electron diffraction and optical spectroscopy, we simultaneously follow the lattice dynamics and dielectric function in the phase-change material $Ge_2Sb_2Te_5$ during an irreversible state transformation. The dielectric function changes by 30% within 100 fs owing to a rapid depletion of electrons from resonantly bonded states. This occurs without perturbing the crystallinity of the lattice, which heats with a 2-ps time constant. The optical changes are an order of magnitude larger than those achievable with silicon and present new routes to manipulate light on an ultrafast timescale without structural changes.

$Ge_2Sb_2Te_5$ (GST) is the prototypical phase-change material and exhibits the fastest crystallization[7] and amorphization rates[6] measured so far. The crystalline state is electrically conductive and optically opaque whereas the amorphous state lacks long-range order and has a lower electrical conductivity and optical absorption. Understanding the speed of the structural transformation and its relation to the optical properties continues to be a significant research topic for improving the design of materials for future devices.

The conventional pathway for amorphization is to heat the crystalline state above the melting point ($T_m = 615\,^{\circ}C$; ref. 8) to disorder the lattice and then rapidly quench the system to freeze the disorder[9]. However, to explain the speed of amorphization in GST, alternative mechanisms have been proposed. It has been suggested that the Ge ions' coordination changes through an 'umbrella flip' transition, which modifies both the structure and optical properties[10]. As only a subset of bonds would change, this type of mechanism has the potential to be very fast and non-thermal. However, the thermal stability of the umbrella flip model has been questioned,[11] and later work has shown that coordination changes alone are insufficient to explain the observed changes in the optical properties[12,13].

Alternatively, the crystalline–amorphous optical contrast has been explained in terms of resonant bonds in the crystalline state[12,13]. Resonant bonds form in specific crystalline systems in which the electronic orbitals of half-filled *p*-type bands are aligned over next-nearest neighbours. These extended delocalized states give rise to a large dipole matrix-element enhancement of the optical properties that is manifested in the large value of the real part of the dielectric function in the low-energy (<2 eV) region[14]. This enhancement is lost when there is angular disorder between the extended *p*-states, changing the optical properties markedly despite the local (nearest-neighbour) bonding remaining relatively unperturbed, as is the case for amorphous GST (refs 13,15).

The sensitivity of resonant bonds to bond alignment has also generated ideas for non-thermal transformation routes. Simulations have shown that distortions to a subset of bonds in the crystalline state of phase-change materials can trigger collapse to the amorphous state[16]. As thermal heating affects all bonds, selective excitation of specific bonds could be a more efficient route to generate the amorphous phase, and it has been suggested that this may occur during the photo-driven phase transformation.

Here, we provide direct measurements of the structural and optical dielectric properties during the photo-triggered amorphization of GST using a combination of time-resolved femtosecond optical spectroscopy and electron diffraction in the single-shot regime. This combination allows us to unambiguously disentangle the electronic and structural contributions to the optical properties. In the first few picoseconds, we observe a separation of the optical properties from the structural state. Changes in the dielectric function, very similar to the equilibrium changes between crystalline and amorphous states, are observed immediately after excitation, consistent with a loss of resonant bonding. However, on this timescale the lattice is still cold and long-range order is still present. Permanent switching to the amorphous state is a slower process, dictated by the thermal response of the lattice that occurs only when the induced temperature jump is sufficient to melt the film.

Figure 1a shows the permanent change induced in GST by single 35-fs pulses at 800-nm central wavelength and 30-nm bandwidth. We find that an incident fluence greater than $F_{TH} = 14\,mJ\,cm^{-2}$ leads to amorphization of the 30-nm-thick crystalline thin-film samples, and fluences above $32\,mJ\,cm^{-2}$ result in ablation. Amorphization was confirmed by a Raman analysis of the pumped region, which is shown in the Supplementary Information together with the sample preparation and characterization techniques.

[1]Fritz-Haber-Institut der Max-Planck-Gesellschaft, Faradayweg 4-6, D-14195 Berlin, Germany. [2]ICFO-Institut de Ciències Fotòniques, Mediterranean Technology Park, 08860, Castelldefels, Barcelona, Spain. [3]ICREA-Institució Catalana de Recerca i Estudi Avançats, 08015 Barcelona, Spain. [4]SUTD-Singapore University of Technology & Design, 8 Somapah Road, 487372 Singapore, Singapore. †These authors contributed equally to this work. *e-mail: ernstorfer@fhi-berlin.mpg.de; simon.wall@icfo.es

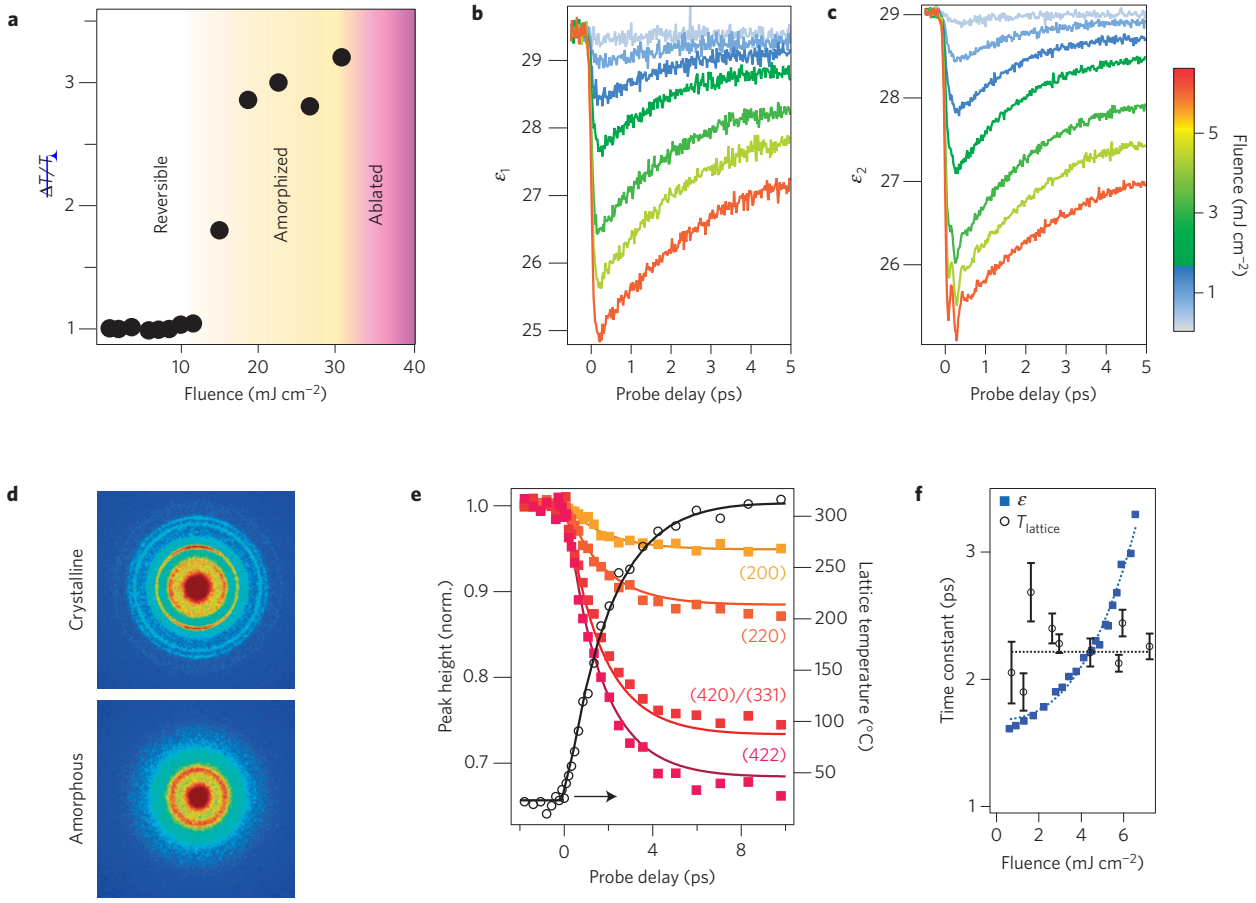

Figure 1 | Below-threshold dynamics in crystalline GST. a, Permanent change in sample transmission measured minutes after irradiation by single femtosecond laser pulses. The sample amorphizes with a single pulse for $F > F_{TH} = 14\ mJ\ cm^{-2}$ and ablation occurs for $F > 32\ mJ\ cm^{-2}$. **b**,**c**, Dynamics of the real (**b**) and imaginary (**c**) parts of the dielectric function at 1.5 eV show a prompt decrease and exponential recovery after photoexcitation. **d**, Static diffraction patterns of crystalline and amorphous states recorded with femtosecond electron bunches at 92 keV. **e**, Evolution of several diffraction peaks after excitation with $5.8\ mJ\ cm^{-2}$ and the extracted temperature change. The temperature dynamics are fitted with a single 2.2-ps exponential rise. **f**, The time constant from the diffraction and the optical data for various fluences showing the recovery time of ε is sensitive to the fluence, whereas the heating dynamics are independent of fluence.

The dynamics of the crystalline state for fluences below F_{TH} are shown in Fig. 1b–f. These measurements were made using conventional pump–probe techniques at low repetition rates (<100 Hz) to avoid cumulative heating in the sample. Although the single-shot transformation threshold was $14\ mJ\ cm^{-2}$, the maximum fluence in the reversible regime was limited to approximately $7\ mJ\ cm^{-2}$, as a gradual transformation of the sample over several minutes was observed for higher fluences. We simultaneously measure the time-dependent changes in the transmitted and reflected light at 800 nm, which we use to calculate the time-dependent dielectric function shown in Fig. 1b,c. Electron diffraction patterns (Fig. 1d) were measured in transmission with 92-keV femtosecond electron pulses[17] and the diffraction peaks were fitted to obtain their evolution as a function of time delay (Fig. 1e). All measurements were performed at near-normal incidence, and further details can be found in the Methods and Supplementary Information.

For below-threshold excitation we observe three phenomena: ~~1.~~ photoexcitation triggers a pronounced and prompt decrease in both the real (ε_1) and imaginary (ε_2) parts of the dielectric function followed by an exponential recovery, whereas the lattice shows a slow decrease in diffraction intensity; an oscillatory response modulates ε_2; the recovery time of the optical signal increases with increasing pump fluence, whereas the lattice dynamics are independent of fluence (Fig. 1f).

Optically exciting GST at 800 nm generates free carriers by interband transitions. The enhanced free-carrier density increases the plasma frequency, which decreases ε_1 and increases ε_2. When observed at 800 nm, these effects are usually small[18]. However, the optical response of crystalline GST shows a large decrease in both ε_1 and ε_2 and is thus not described by the response of free carriers. Instead, we attribute this effect to a photobleaching of electrons from resonantly bonded states, as the primary effect resulting from the loss of resonant bonding is a large decrease in ε (ref. 12). The initial decrease of ε_1 and ε_2 scales linearly with pump intensity; however, the recovery time, which is the same for ε_1 and ε_2, increases nonlinearly as shown in Fig. 1f. Photoexcitation also generates oscillations that perturb only ε_2, corresponding to coherent Raman-active vibrations (see the Supplementary Information for a comparison of the spectra)[19]. As the Raman-active modes do not significantly perturb ε_1, we conclude that they do not particularly perturb the resonant bonds.

We now consider the evolution of the diffraction peaks following laser excitation shown in Fig. 1e. The temporal behaviour can be explained by an increase in mean-square displacement of the atoms around their equilibrium position. If we assume that the lattice vibrations are thermal at all times, the system is describable by a time-dependent temperature, which can be obtained through an analysis of the Debye–Waller B-factor[20]. The extracted temperature evolution is also shown in Fig. 1e and can be fitted ~~using~~ a single

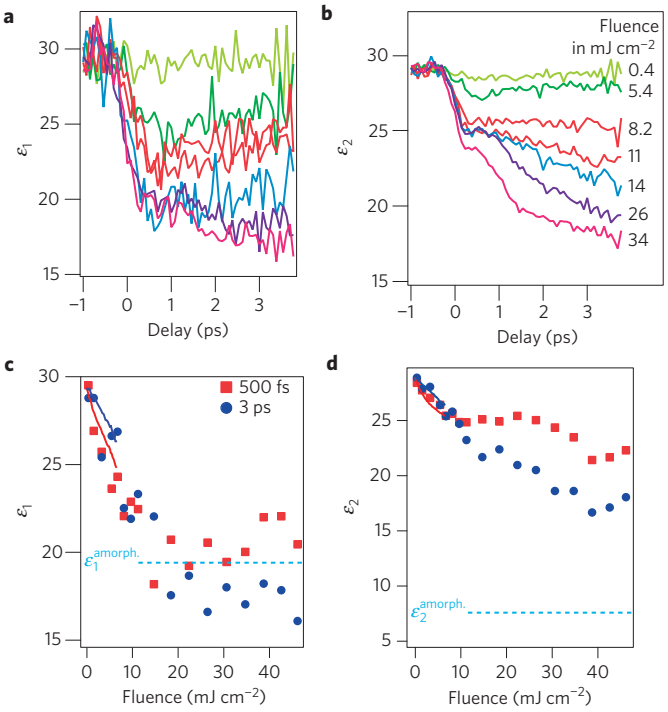

Figure 2 | Dynamics of the dielectric function during amorphization. **a**,**b**, Time dependence of the real (**a**) and imaginary (**b**) parts of the dielectric function ε, labelled by the incident fluence in mJ cm^{-2}. As F_{TH} is approached, ε_1 saturates, but ε_2 shows a further slow dynamic. Increasing the fluence of the pump pulse above the ablation threshold ($F > 32$ mJ cm^{-2}) does not cause a significant change in either dynamic. **c**,**d**, The power dependence of the real and imaginary parts of the dielectric function respectively at 500 fs and 3 ps. ε_1 saturates at the value of the dielectric function in the amorphous phase (horizontal dashed line) above F_{TH}. This occurs within the time resolution and shows little subsequent evolution. ε_2 saturates at short delays at a value far from the equilibrium amorphous value, but continues to evolve on longer timescales. Solid lines show low fluence data from Fig. 1b,c.

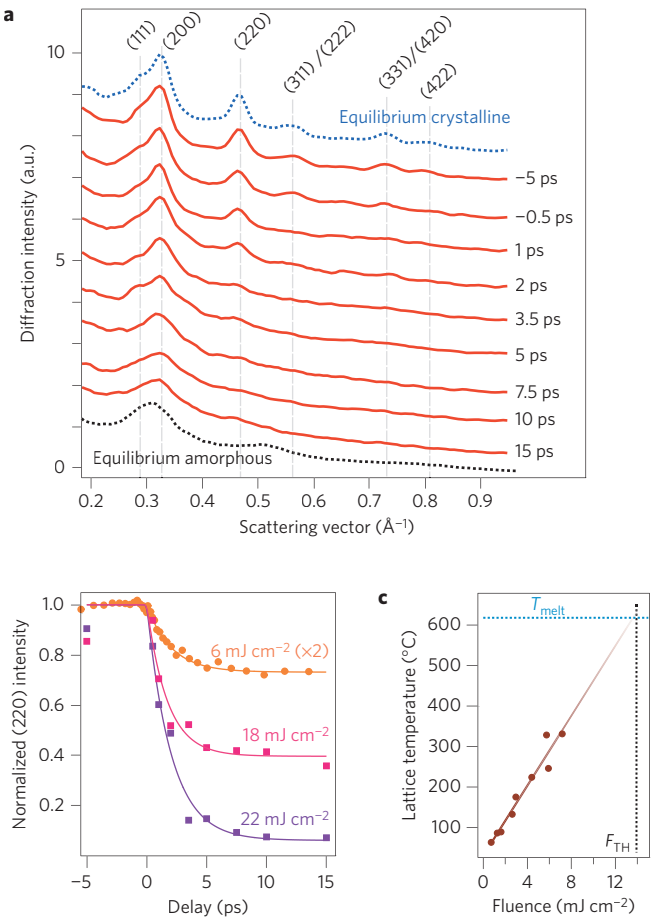

Figure 3 | Structural dynamics during amorphization. **a**, Raw radially integrated diffraction patterns measured in the single-shot regime for a pump fluence of 22 mJ cm^{-2} at several time delays. The diffraction orders are labelled, with multiple labels indicating that diffraction orders overlap. Contrast between the (200) and (220) peaks is lost by approximately 5 ps. **b**, The time evolution of the (220) diffraction peak. The same time profile is obtained using the below-threshold data of the lattice heating with a time constant of 2.2 ps to fit the above-threshold response by scaling the amplitude. This demonstrates that the loss of long-range order occurs by thermal melting. **c**, Fluence dependence of the calculated temperature after laser excitation from the below-threshold data. The straight line is a linear fit to the data.

exponential rise with a time constant of 2.2 ps (see Methods for details). The good agreement between the fitted diffraction peaks based on a thermal lattice and the measured data suggests that the lattice is, to good approximation, thermal.

Interestingly, unlike the optical signal, the lattice-heating time constant is independent of fluence (Fig. 1f). This difference indicates that the recovery of the dielectric function cannot be simply attributed to electrons thermalizing with the lattice. Instead, it can be understood in terms of resonant bonding. As the lattice heats, ions fluctuate further from their equilibrium positions, disrupting the *p*-orbital alignment. As lattice disorder makes bond alignment over an extended number of lattice sites unlikely, reformation of resonant bonding becomes less probable and the recovery time increases as the lattice heats.

When the pump power is increased above F_{TH}, single pump pulses induce irreversible changes in the sample, and conventional pump–probe techniques are not suitable to study the dynamics. Instead the optical measurements harness a chirped probe pulse and spectral encoding to map the temporal response onto the frequency domain, allowing us to measure the initial 3-ps dynamics with 100-fs time resolution using only a single laser pulse[21]. Electron diffraction images were taken with single electron bunches, and the dynamics were measured by moving the sample to a fresh spot for each time point. Technical details are given in the Supplementary Information.

Figure 2 shows the dynamics of the dielectric function for a range of fluences that cover amorphization and even ablation regimes. The amplitude of the initial drop of ε_1 increases with increasing excitation fluence ~~until~~ the threshold fluence. At this point, ε_1 has decreased by 30% within 100 fs and does not respond to further increases in pump fluence nor evolve in time. Remarkably, the saturated value reached on the femtosecond timescale is the same as that of the amorphous phase. As resonant bonds are not present in the amorphous phase, the appearance of properties similar to the amorphous state indicates that the resonant-bonding contribution to the dielectric function has been completely suppressed within these 100 fs. ε_2 also shows a similar saturation as a function of fluence at short times, but at a value that is still far from that of the amorphous phase. Unlike ε_1, however, it continues to evolve in time, and large changes occur on a slower timescale.

The ultrafast saturation in ε_1 to the amorphous phase value suggests that the resonantly bonded states have been completely suppressed on a sub-picosecond timescale as would be expected for a non-thermal phase transition. Femtosecond electron diffraction, however, reveals that the lattice responds on a slower timescale. Figure 3a shows that the crystalline structure persists for several

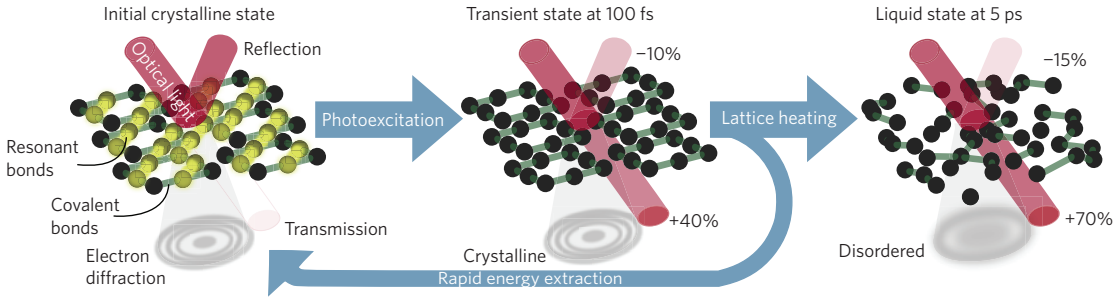

Figure 4 | Schematic of the ultrafast transformation pathway. Crystalline GST exists with resonant bonds (yellow, subset shown for clarity) that dictate the optical properties. Ultrafast photoexcitation forms a new transient state by removing the resonant bonds and changing the optical properties before ionic motion has occurred. Transfer of the electron energy to the covalent backbone causes lattice heating, which thermally melts the long-range order after several picoseconds. Subsequent thermalization determines the final material state. Rapid energy extraction during the transient state could prevent thermal melting and enable the restoration of the resonantly bonded state quickly.

picoseconds after photoexcitation, and the complete loss of long-range order is observed after approximately 5–10 ps. Figure 3b shows the temporal evolution of the (220) peak for 3 fluences. The temporal evolution above threshold can be fitted by scaling the amplitude of the intensity change and keeping the timescales constant, indicating that the above-threshold lattice dynamics are described by the same thermal process. Figure 3c shows that the final lattice temperature achieved for below-threshold excitation increases linearly with excitation fluence. Although this linearity is not expected to continue when the state changes, extrapolating up to the threshold reveals a good agreement between the melting temperature and the transformation fluence.

The unique combination of measurements presented here allows us to obtain a microscopic picture of the initial steps in the photoinduced amorphization process in phase-change materials, which is schematically depicted in Fig. 4. Femtosecond optical excitation directly removes electrons from resonantly bonded states as evidenced by the immediate decrease in the dielectric function and the saturation of ε_1 at the amorphous-state value. This non-thermal femtosecond change in the optical properties does not coincide with a change in crystallinity and represents a previously unobserved non-equilibrium state of GST.

This non-equilibrium state is lost during lattice heating. Heating occurs with a 2.2-ps exponential time constant that is dictated by the rate of energy transfer from electrons to vibrations of the covalently bonded backbone of the crystalline lattice[16]. When photoexcited with 800-nm light to the level needed to completely suppress resonant bonding, there is also sufficient energy deposited to melt the crystal on thermalization. Once melted, the final state obtained depends on how quickly the heat is extracted from the liquid. We find no evidence for any non-thermal lattice dynamics, in contrast to observations in other materials[22–25] and thus photoexcitation at 800 nm is unable to affect the lattice non-thermally as described in ref. 16. Such dynamics may be observable at higher excitation fluences in the ablation regime, which is of limited interest for practical reasons. Our combination of optical and structural probing allows us to deduce that structural amorphization is much slower than the 130–200 fs suggested from optical transmission data alone[26]. Phase transformation through the molten state is also consistent with previous time-resolved measurements on photoinduced crystallization in another phase-change material, GeSb, in which crystallization occurred after the amorphous state was melted[27].

The observation that resonant bonds can be controlled rapidly and non-thermally, apart from the crystalline lattice, represents a new understanding of the phase transformation in GST. Switching the optical properties of GST is no longer dictated by the absolute atomic arrangement, but rather only stabilized by it. Without the complete depopulation of the resonantly bonded state, we achieve reversible modulations of the dielectric function ~~of up to 13%~~, more than an order of magnitude larger than observed in silicon photoswitches[28]. By extracting the energy used to depopulate the resonant bonds before the lattice heats above the melting temperature, as suggested in Fig. 4, an ultrashort-lived state with 30% change in the dielectric function may be achieved. Energy extraction could be realized in nanostructured devices by rapid transfer of the photoexcited carriers, both electrons and holes, into a metal or semimetal, for instance in layered heterostructures composed of GST and graphene or few-layer graphite. Additionally, efficient vibrational coupling of nanoscale GST to the ~~surrounding~~ will limit the maximum lattice temperature, and resonant bonds could re-establish and recover the crystalline-state optical properties on the few-picosecond timescale. As the structural transition limits the lifetime of GST-based devices, achieving optical contrast without the structural change is a major advantage and will improve cyclability. We expect that the transient optical changes will be even larger at telecommunication wavelengths, as the infrared spectral region has a greater sensitivity to changes in resonant bonding; thus, the ability to harness the ultrafast optical contrast of phase-change materials without structural transition suggests a new avenue to high-speed optical modulators[29] for communications and computations.

Methods

Methods and any associated references are available in the online version of the paper.

Received 3 March 2015; accepted 22 June 2015;
published online XX Month XXXX

References

1. Wuttig, M. & Yamada, N. Phase-change materials for rewriteable data storage. *Nature Mater.* **6,** 824–832 (2007).
2. Wuttig, M. Phase-change materials: Towards a universal memory? *Nature Mater.* **4,** 265–266 (2005).
3. Hosseini, P., Wright, C. D. & Bhaskaran, H. An optoelectronic framework enabled by low-dimensional phase-change films. *Nature* **511,** 206–211 (2014).
4. Rudè, M. *et al.* Optical switching at 1.55 μm in silicon racetrack resonators using phase change materials. *Appl. Phys. Lett.* **103,** 141119 (2013).
5. Rios, C., Hosseini, P., Wright, C. D., Bhaskaran, H. & Pernice, W. H. P. On-chip photonic memory elements employing phase-change materials. *Adv. Mater.* **26,** 1372–1377 (2014).
6. Loke, D. *et al.* Ultrafast phase-change logic device driven by melting processes. *Proc. Natl Acad. Sci. USA* **111,** 13272–13277 (2014).
7. Loke, D. *et al.* Breaking the speed limits of phase-change memory. *Science* **336,** 1566–1569 (2012).
8. Kolobov, A. V. *et al.* Liquid $Ge_2Sb_2Te_5$ studied by extended X-ray absorption. *Appl. Phys. Lett.* **95,** 241902 (2009).

9. Kohara, S. *et al.* Structural basis for the fast phase change of $Ge_2Sb_2Te_5$: Ring statistics analogy between the crystal and amorphous states. *Appl. Phys. Lett.* **89,** 201910 (2006).
10. Kolobov, A. V. *et al.* Understanding the phase-change mechanism of rewritable optical media. *Nature Mater.* **3,** 703–708 (2004).
11. Lang, C., Song, S., Manh, D. & Cockayne, D. Building blocks of amorphous $Ge_2Sb_2Te_5$. *Phys. Rev. B* **76,** 054101 (2007).
12. Shportko, K. *et al.* Resonant bonding in crystalline phase-change materials. *Nature Mater.* **7,** 653–658 (2008).
13. Huang, B. & Robertson, J. Bonding origin of optical contrast in phase-change memory materials. *Phys. Rev. B* **81,** 081204 (2010).
14. Lucovsky, G. & White, R. Effects of resonance bonding on the properties of crystalline and amorphous semiconductors. *Phys. Rev. B* **8** (1973).
15. Caravati, S., Bernasconi, M. & Parrinello, M. First principles study of the optical contrast in phase change materials. *J. Phys. Condens. Matter* **22,** 315801 (2010).
16. Kolobov, A. V., Krbal, M., Fons, P., Tominaga, J. & Uruga, T. Distortion-triggered loss of long-range order in solids with bonding energy hierarchy. *Nature Chem.* **3,** 311 (2011).
17. Waldecker, L., Bertoni, R. & Ernstorfer, R. Compact femtosecond electron diffractometer with 100 keV electron bunches approaching the single-electron pulse duration limit. *J. Appl. Phys.* **117,** 044903 (2015).
18. Huang, L., Callan, J., Glezer, E. & Mazur, E. GaAs under intense ultrafast excitation: Response of the dielectric function. *Phys. Rev. Lett.* **80,** 185–188 (1998).
19. Zeiger, H. *et al.* Theory for displacive excitation of coherent phonons. *Phys. Rev. B* **45,** 768–778 (1992).
20. Caravati, S., Bernasconi, M., Kühne, T. D., Krack, M. & Parrinello, M. First principles study of crystalline and amorphous $Ge_2Sb_2Te_5$ and the effects of stoichiometric defects. *J. Phys. Condens. Matter* ~~**22,** 399801–399801~~ (2010).
21. Shkrob, I. A., Oulianov, D. A., Crowell, R. A. & Pommeret, S. Frequency-domain 'single-shot' ultrafast transient absorption spectroscopy using chirped laser pulses. *J. Appl. Phys.* **96,** 25 (2004).
22. Sciaini, G. *et al.* Electronic acceleration of atomic motions and disordering in bismuth. *Nature* **458,** 56–59 (2009).
23. Siders, C. W. *et al.* Detection of nonthermal melting by ultrafast X-ray diffraction. *Science* **286,** 1340–1342 (1999).
24. Lindenberg, A. M. *et al.* Atomic-scale visualization of inertial dynamics. *Science* **308,** 392–395 (2005).
25. Harb, M. *et al.* Electronically driven structure changes of Si captured by femtosecond electron diffraction. *Phys. Rev. Lett.* **100,** 155504 (2008).
26. Takeda, J., Oba, W., Minami, Y., Saiki, T. & Katayama, I. Ultrafast crystalline-to-amorphous phase transition in $Ge_2Sb_2Te_5$ chalcogenide alloy thin film using single-shot imaging spectroscopy. *Appl. Phys. Lett.* **104,** 261903 (2014).
27. Callan, J. *et al.* Ultrafast laser-induced phase transitions in amorphous GeSb films. *Phys. Rev. Lett.* **86,** 3650–3653 (2001).
28. Kampfrath, T. *et al.* Ultrafast adiabatic manipulation of slow light in a photonic crystal. *Phys. Rev. A* **81,** 043837 (2010).
29. ~~Rude),~~ M. *et al.* Ultrafast broadband tuning of resonant optical nanostructures using phase change materials. Preprint at http://arxiv.org/abs/1506.03739 (2015).

Acknowledgements

T.A.M. acknowledges financial support through the Marie Curie COFUND project and Spanish Ministry of Economy and Competitiveness (MINECO). R.B. thanks the Alexander von Humboldt Foundation for financial support. V.P. acknowledges financial support from MINECO and the 'Fondo Europeo de Desarrollo Regional' (FEDER) through grant TEC2013-46168-R. R.E. acknowledges fruitful discussions with M. Wuttig and ~~financial support~~ from the Max Planck Society. S.W. acknowledges financial support from Ramon y Cajal program RYC-2013-14838 and Marie Curie Career Integration Grant PCIG12-GA-2013-618487. V.P. and S.W. acknowledge support from Fundació Cellex.

Author contributions

S.W., L.W. and R.E. initiated the project. T.A.M. and S.W. performed the multi-shot optical measurements. S.W., L.W. and T.A.M. performed the single-shot optical measurements. L.W. and R.B. performed the time-resolved diffraction measurements. M.R. fabricated samples, which were characterized by M.R., T.A.M. and J.O. All authors provided input to the interpretation of the data and writing the manuscript.

Additional information

Supplementary information is available in the online version of the paper. Reprints and permissions information is available online at www.nature.com/reprints. Correspondence and requests for materials should be addressed to R.E. or S.W.

Competing financial interests

The authors declare no competing financial interests.

Methods

Sample preparation. For optical measurements, 30-nm GST films were grown on fused-silica substrates by radiofrequency co-sputtering from two stoichiometric targets of GeTe and Sb_2Te_3 in an Ar atmosphere. The as-deposited film is amorphous and its stoichiometry is confirmed to be close to $Ge_2Sb_2Te_5$ by energy-dispersive X-ray measurements (accuracy of 5%). ~~Ten nanometre~~ Si_3N_4 capping layer films were grown by reactively d.c. sputtering from a Si target for 10 min using a mixture of Ar and N_2 as a process gas. The capping layer is used to prevent oxidation of the GST layer. Crystallization of the GST was achieved by annealing the sample on a hot plate at 200 °C for 1 h using a heating rate of 10 °C min^{-1}, and the final state was characterized by Raman and optical spectra and is plotted in the Supplementary Information.

Determination of the dielectric function. The dielectric function was measured using broadband ellipsometry. The values obtained were in excellent agreement at 800 nm with those found using a transfer matrix method to invert reflection (R) and transmission (T) data measured at normal incidence on the same films.

Time-dependent measurements measure $\Delta R/R$ and $\Delta T/T$. We use the static R and T values to convert the transients into the absolute value of R and T as a function of time. These values were then inverted using the transfer matrix method to recover the complex dielectric function. We assume coherent reflections from the GST and Si_3N_4 layers ($n_{Si_3N_4} = 1.99622$) and incoherent reflections from the backside of the SiO_2 substrate ($n_{SiO_2} = 1.45332$). Raw reflection and transmission data and further details can be found in the Supplementary Information.

Single-shot optical technique. Single-shot measurements were performed using a spectral-encoding technique[21]. A 35-fs, 800-nm pulse passes twice through a block of glass, stretching the pulse to approximately 12 ps with a linear chirp. The pulse is incident on the sample at near-normal incidence and, together with a reference signal taken before the sample, the transmitted and reflected signals are focused into separate fibres and are individually imaged onto a CCD (charge-coupled device) camera in an imaging spectrometer.

The linear chirp results in each colour in the probe interacting with the sample at a different time. If we assume that the resulting $\Delta R/R$ and $\Delta T/T$ due to the time-dependent dielectric function is independent of the probe frequency within our laser spectrum, we can extract the time-dependent signal. The details of the temporal calibration are found in the Supplementary Information.

Femtosecond electron diffraction. Diffraction experiments use a pump–probe scheme with an 800-nm 35-fs pump pulse and a short electron bunch as a probe of the structural state. We create short electron pulses by photo-emission of electrons from a photocathode and acceleration to a kinetic energy of 92 keV in a static electric field. The electron bunch then diffracts off the sample that is placed shortly behind the anode, and a two-dimensional diffraction image is recorded with an electron camera. For the employed bunch charge, the electron pulse duration on the sample is estimated to be 150 fs from measurements made on Al foils.

Owing to the high scattering cross-section of electrons with matter, the diffraction experiment requires thin, freestanding films of the sample under study. To ensure comparability to the optical experiments, we use a sandwich geometry consisting of a 30-nm-thick film of GST with a 10-nm-thick capping layer of Si_3N_4 on the front side and replace the glass substrate with yet another 10-nm-thick layer of Si_3N_4. The films are transferred to a large area ($20 \times 20\ mm^2$) grid with $190 \times 190\ \mu m^2$ holes etched from a silicon wafer. The sample can be translated in three directions in the vacuum chamber and its tip and tilt can be controlled by two additional motors to ensure parallel movement to the stages. In the single-shot experiment, a fresh piece of sample can be supplied for each laser shot without changing the temporal overlap of pump and probe.

Electron diffraction experiments with reversible excitation have been performed at different repetition rates to avoid temperature offsets at negative delay times due to accumulated heating by multiple pump pulses. By comparison of diffraction images at negative pump–probe delays with measurements without pump laser, the repetition rate was lowered until no offset could be observed.

Electron diffraction data analysis and lattice temperature calculation. We record two-dimensional diffraction images with a phosphor screen fibre-coupled to a CMOS chip (TVIPS TemCam-F416). The appearance of weak texture in the Debye–Scherrer rings has been observed in some samples (see Fig. 1d), but has not shown to influence the structural dynamics. The recorded images are thus integrated angularly in both single-shot and reversible measurements to obtain radial averages. From these, the relative peak heights can be determined by fitting and subtracting a background (Lorentzian + fourth-order polynomial) and fitting pseudo-Voigt line profiles to the peaks for each time delay.

A Debye–Waller type analysis of the diffraction data was used to calculate a lattice temperature from the relative diffraction peak heights. This analysis relies on the assumption that the phonons are close to a thermal distribution at all delay times and that phonon modes do not shift through photoexcitation, which we find to be valid.

The relative intensity of a peak with scattering vector S at a temperature T with respect to the initial reference temperature, T_0, is given by:

$$I_{rel,S}[T(t)] = \exp(S^2(B(T_0) - B(T(t))))$$

~~with~~ $B(T)$ ~~being the~~ Debye–Waller B factor ~~for the given temperature~~ that is given in ref. 20. Equivalently, the relative intensity of a Bragg peak with scattering vector S of a sample in a thermal state can be written in a form that depends only on temperature:

$$-\frac{\ln(I_{rel,S}(t))}{S^2} = B(T(t)) - B(T_0)$$

Plotted in this form, the relative intensities of all Bragg peaks lie on top of each other. This indicates that the phonon distribution is isotropic and no strong coupling to specific modes is present. We therefore calculate a lattice temperature $T(t)$ from our data, which is obtained by averaging the peak intensities in this form and numerically solving the equation. This temperature $T(t)$ is used to recalculate the expected evolution of the individual peaks, and it is this calculated peak height as a function of temperature that is plotted with solid lines in Fig. 1e.

Finally, $T(t)$ is fit~~ted~~ by the following ~~fit~~ function:

$$T(t) = T_0 + \Delta T_1 \left(1 - \exp\left(-\frac{t}{\tau_1}\right)\right) - \Delta T_2 \left(1 - \exp\left(-\frac{t}{\tau_2}\right)\right), \quad t > 0$$

where T_0 is initial lattice temperature, ΔT_1 is the temperature increase resulting from the thermalization of the electrons and the lattice and τ_1 is the heating rate, plotted in Fig. 1f. ΔT_2 is the amplitude of cooling, and τ_2 is the cooling rate, due to heat diffusion into the Si_3N_4 capping layers. τ_2 was found from long time scans of the diffraction signal and was found to be 100 ps. Heat diffusion resulted in a cooling of the film by 20–50% of the initial heating at 100 ps. The values of ΔT_1 found in the Debye–Waller analysis are in good agreement with expected temperature rises using values of the static heat capacity of 0.25 J g^{-1} K^{-1} and the absorbed energy densities of the GST films[30].

References

30. Kuwahara, M. *et al.* Temperature dependence of the thermal properties of optical memory materials. *Jpn. J. Appl. Phys.* **46,** 3909–3911 (2007).

Queries for NPG paper nmat4359

Page 1

Query 1:
Please note that reference numbers are formatted according to style in the text, so that any reference numbers following a symbol or acronym are given as 'ref. XX' on the line, whereas all other reference numbers are given as superscripts.

Page 2

Query 2:
'while' changed to 'and' in the sentence 'The sample amorphizes ..' in the caption of figure 1a, to avoid non-time-related use of the former; please check, and amend if necessary. Also, please amend the caption of f to define the error bars.

Query 3:
Text amended here to avoid the numbered list. Please check, and amend if necessary.

Query 4:
'oscillations which only perturb' changed to 'oscillations that perturb only' here, according to style, to use 'that' as a defining pronoun (and 'which' to introduce a further description), and to place 'only' directly in front of the word/phrase it modifies. Please check.

Page 4

Query 5:
Should 'surrounding' be 'surroundings' here, or is a word/phrase missing after 'surrounding'?

Page 5

Query 6:
Please provide volume and page range for ref. 14.

Query 7:
Please provide page range/article id for refs 16, 21.

Query 8:
Please make sure that ref. 29 has not been published in any journal.

Page 6

Query 9:
Can the text here be amended to avoid repetition of 'given'?